

The Luminosity Function of M3¹

R.T. Rood², E. Carretta³, B. Paltrinieri⁴, F. R. Ferraro^{5,6}

F. Fusi Pecci^{6,7}, B. Dorman⁸,

A. Chieffi⁹, O. Straniero¹⁰, R. Buonanno¹¹

ABSTRACT

We present a high precision, large sample luminosity function (LF) for the Galactic globular cluster M3. With a combination of ground based and *Hubble Space Telescope* data we cover the entire radial extent of the cluster. The observed LF is well fit by canonical standard stellar models from the red giant branch (RGB) tip to below the main sequence turnoff point. Specifically, neither the RGB LF-bump nor subgiant branch LF indicate any breakdown in the standard models. On the main sequence we find evidence for a flat initial mass function and for mass segregation due to the dynamical evolution of the cluster.

Subject headings: globular clusters: individual (M3) — stars: red giant— —stars: evolution

¹Based in part on observations with the NASA/ESA *Hubble Space Telescope*, obtained at the Space Telescope Science Institute, which is operated by AURA, Inc., under NASA contract NAS5-26555

²Astronomy Dept, University of Virginia, P.O.Box 3818, Charlottesville, VA 22903-0818; rtr@virginia.edu

³Osservatorio Astronomico di Padova, vicolo dell'Osservatorio 5, 35122 Padova, ITALY; carretta@astrpd.pd.astro.it

⁴Istituto di Astronomia-Universitá "La Sapienza", via G.M. Lancisi 29, I-00161 Roma, Italy; barbara@coma.mporzio.astro.it

⁵European Southern Observatory, Karl Schwarzschild Strasse 2, D-85748 Garching bei München, Germany

⁶Osservatorio Astronomico di Bologna, via Ranzani 1, 40126 Bologna, ITALY; ferraro,flavio@astbo3.bo.astro.it

⁷Stazione Astronomica di Cagliari, 09012 Capoterra, ITALY

⁸Laboratory for Astronomy & Solar Physics, Code 681, NASA/GSFC, Greenbelt MD 20771; dorman@veris.gsfc.nasa.gov

⁹Istituto di Astrofisica Spaziale-CNR, 00044 Frascati, ITALY; alessandro@altachiara.ias.rm.cnr.it

¹⁰Osservatorio Astronomico di Collurania, 64100 Teramo, ITALY; straniero@astrte.te.astro.it

¹¹Osservatorio Astronomico di Roma, 00040 Monte Porzio, ITALY; buonanno@coma.mporzio.astro.it

1. Introduction

One of the classical tests of stellar evolutionary calculations is through the comparison of theoretical and observed stellar luminosity functions (LFs) of globular clusters (e.g., Renzini & Fusi Pecci 1988). The LF for the stars below the main sequence turn-off (MSTO) can be related to the stellar initial mass function and be used as a probe of stellar dynamics within a cluster. The LF of stars after the MSTO depends primarily on the rate of evolution and provides a direct and straight-forward test of evolutionary calculations. Basically the post-MSTO LF measures the development of the hydrogen burning shell and its progression through the star. Features in the observed LF can be related to interior structure. For example, as first noted by Iben (1968), when the H-burning shell advances through the composition discontinuity left by the maximum penetration of convective envelope, the luminosity briefly decreases. This leads to the so-called LF bump. More subtle observables are also present: the slope of the LF below and above the LF bump are different because the H-burning shell is in the first case passing through a region of varying H abundance and later through a region of constant H (Rood & Crocker 1985, Fusi Pecci et al. 1990). A breakdown in *canonical* stellar evolution theory (Renzini & Fusi Pecci 1988) can affect the LF in the region of the subgiant branch (SGB).¹² Examples include extra energy transport by Weakly Interacting Massive Particles (WIMPs) (Faulkner & Swenson 1993) or the gravitational settling of helium (Proffit & VandenBerg 1991, Castellani et al. 1997, Straniero et al. 1997), both of which affect the cluster age calibration.

To explore short evolutionary phases or to search for the small changes in the LF produced by reasonable modifications to the canonical models requires large samples. Indeed, to explore phenomena like those cited above, such large samples are required that photometry must extend to the crowded inner parts of clusters. To be useful in constructing

a LF, photometric samples must be complete and accurate—a requirement which has come into conflict with the necessity of working near cluster cores. Adequate samples to identify the LF-bump were first obtained for 47 Tuc by King, DaCosta & Demarque (1985) and for 11 other clusters by Fusi Pecci et al. (1990) (see Cassisi & Salaris 1997 for a review). At lower luminosities LF studies have produced some puzzling results. Stetson (1991) in a LF formed from combined data from the low metallicity clusters M68, M92, and NGC 6397 found an excess of stars on the SGB just above the MSTO. Bolte (1994) found a similar result for M30 which has been confirmed by Bergbusch (1996), Guhathakurta et al. (1998) and Sandquist et al. (1999). This excess was especially intriguing because that was the “signature” expected if WIMP energy transport was important (Faulkner & Swenson 1993). However Sandquist et al. (1996) in the largest sample LF obtained to date did not find a similar result for the somewhat more metal rich cluster M5.

Clearly larger and better LFs are desirable, and these are now possible with the *Hubble Space Telescope (HST)* which has the capability to obtain photometry near cluster centers. While very large *HST* samples of fainter stars can be obtained, the small field of view limits the number of evolved stars which can be observed. However, the combination of ground based photometry of the outer cluster and *HST* data can yield a large sample LF which spans the range of cluster stellar luminosities. In this paper we present such an LF obtained for the cluster M3 (NGC 5272). This is the largest, most precise, and most complete LF yet obtained for a globular cluster.

2. HST-WFPC2 Data Sample

2.1. Observations and Data Analysis

The observations were obtained April 25, 1995 as part of the *HST* program GO5496 (P.I. F. Fusi Pecci), the first of our programs devoted to testing the theoretical models using luminosity functions of a set of Galactic Globular Clusters with different metallicity.

A set of exposures was secured through UV (F255W and F336W) and optical filters (F555W and F814W). Preliminary results on UV data has been already presented in Ferraro et al. (1997a) and Laget et al. (1998); here we will report on results obtained using only the *V* and *I* exposures. Total exposure times were 400 sec in *V* (F555W) and 560 sec in *I* (F814W);

¹²The *canonical* assumptions include the neglect of phenomena like rotation, non-convective matter transport, etc. in stellar model calculations. Some of these are certainly present in real stars, but they are very difficult to include in calculations. This leads to two approaches to dealing with non-canonical phenomena: one is to try to model the phenomenon ordinarily in a simplistic way requiring the introduction of free parameters. The other is to make the most stringent possible comparison between observations and canonical models—the approach we adopt here.

each exposure is listed in Table 1 by Ferraro et al. (1997a).

The initial data analysis (including bias, dark and flat-field corrections) was made through the standard *HST* pipeline. A master unsharp mask image for each filter was made using MIDAS to register all the long-exposure images, yielding a median frame with cosmic rays statistically eliminated. The search of the individual star components was made on the V median frame, following the usual procedure with ROMAFOT (Buonanno et al. 1983). Then we performed the PSF fitting on each individual frame separately using a Moffat function plus a numerical map of the residuals to better account for the contribution of the stellar PSF wings. The average instrumental magnitudes for each star were transformed to the standard Johnson V and I system using the Holtzmann et al. (1995) recipes. The magnitudes thus obtained were eventually shifted to match the independent zero-point calibration adopted in Ferraro et al. (1997b, hereafter M3CCD). The V , $V - I$ CMD for the HST global sample is shown in Figure 1.

Special care has been devoted to ensure that the effects of blends (and crowding) do not significantly alter the derived LF. The effects of blending can be quite problematic in CMDs of dense regions of globular clusters. On the main sequence, blended stars can potentially be mistaken for binary stars, while on the subgiant branch they be shifted erroneously to brighter bins. Blends can mimic incompleteness by shifting the two stars off the main loci such that they are dropped from the LF. To minimize these effects suspected blended objects with multiple stellar components lying off the main branches of the CMD were individually examined by eye, exploiting the fully interactive capability of the package ROMAFOT. In this way we were able to check and, if necessary, eliminate spurious objects. The degree to which blends contaminate the final sample can be estimated from the artificial stars tests described below. Some of the artificial stars which were not recovered were lost as blends. Thus the degree of incompleteness at a given level serves as an upper limit to the blend-fraction.

2.2. Completeness

A crucial component in the calculation of an accurate LF is the determination of corrections for incompleteness. In our data crowding is the primary source of incompleteness. Moreover, because of the large gradient in the spatial density of stars present

in our frame, the completeness at any level of magnitude must be determined as a function of the position with respect to the cluster center.

In order to quantify the efficiency in detecting stars as function of the magnitude and the degree of crowding we carried out extensive artificial star tests in the V filter frames, following the procedure described below.

1. Each chip was split into two annular regions centered on the cluster center:

INNER: $r < 50''$ including the entire PC1 field and the innermost part of the three WFC fields;

OUTER: $r > 50''$ covering the outer part of the three WFCs.

M3 is a cluster of moderate central density. With a core radius $r_c = 30''$ (Djorgovski 1993) one would expect the stellar density to be approximately constant across the PC as is apparent from Figure 2. However, the stellar density has dropped appreciably at the outer parts of the WFs. We have adopted $50''$ as a boundary between regions of higher and lower projected stellar density. A map of the WFPC2 field of view is shown Figure 2 with the circle ($at r \sim 50''$) delineating the two regions.

2. A set of artificial stars was generated using the *Tiny Tim* package (Krist 1994), and these were added to the original frames in random positions. In order to avoid a spurious crowding enhancement, the size of the added sample (about 300 total artificial images or ~ 80 for each chip) was $\leq 10\%$ of the total number of stars originally found in each chip. Then the star searching and fitting procedures were repeated on the artificially enriched frames.
3. An artificial star was considered to be “recovered” on the basis of the following criteria:

- the differences in position, Δx , Δy , between the input artificial star and the recovered one are Δx , $\Delta y < 1$ pixel;
- the difference in magnitude, Δmag , is $|\Delta mag| < 0.3$.

The fraction of artificial stars missed during any step of the procedure is a good estimate of the

actual number of stars missed at each magnitude level during the reduction procedure.

4. The completeness factor (Φ) was finally computed as the numbers of stars recovered (N_{rec}) with respect to the number of stars simulated (N_{sim}) during each trial. The final value of Φ has been obtained as an average of 3–6 independent trials for each magnitude bin (0.2 mag width) in each of the two regions (INNER and OUTER).

The result of these tests is summarized in Figure 3a,b. The completeness at the MSTO level ($V \sim 19$) is $> 90\%$ in both the INNER and OUTER regions, thus the star counts up to that level have been corrected by less than 10%. The corrections for completeness were applied separately in each part (inner or outer) of each field (PC, WFCs) so that the total corrected sample properly accounts for the differing degrees of crowding.

2.3. The Mean Ridge Line of the RGB, SGB, and Upper MS

If there were no photometric errors all of the RGB, SGB, and Upper MS stars would lie along a line in the CMD. We approximate this line with a mean ridge line (MRL) which has been determined by an iterative procedure:

1. A first rough selection of stars belonging to the RGB, SGB, MS was performed by eye, excluding the horizontal branch (HB), asymptotic giant branch (AGB), and blue straggler stars (BSS);
2. This preliminary sample was divided into 0.5 mag width bins;
3. For each bin the median $V - I$ color was computed;
4. All stars lying more than $5\sigma_{V-I}$ from the median value was rejected.

Points (3) and (4) of the procedure were iterated until the solution was stable. The resulting MRL points are listed in Table 1. Only about 2% of the sample was rejected in determining the MRL.

Luminosity functions were constructed for each chip by dividing each individual CMD in 0.2 mag bins,

and simply counting all the stars in each bin within $\pm 5\sigma_{V-I}$ of the MRL.

Figure 4 shows a zoom of luminosity function in the Turn-Off region for the total HST sample, before and after correction for completeness. Errors have been computed accordingly to the following relation (see also Bolte 1989):

$$\sigma_{\text{bin}} = \left[\frac{N^{1/2}}{\Phi} + \frac{N \cdot \sigma_{\Phi}}{\Phi^2} \right] \quad (1)$$

where N is the number of stars observed in each bin, Φ is the completeness factor, and σ_{Φ} is the associated error which was determined from the rms of the repeated completeness trials.

3. Matching the Ground-Based Observations: the Global LF

HST data presented here complement the large data set we have obtained for M3 during the last decades. The photographic sample was originally presented by Buonanno et al. (1994) and the CCD ground based data have been discussed by Ferraro et al. (1993, 1997b). The entire photographic sample extends over an area between 2' and 7' from the cluster center. Here we consider a subsample (hereafter referred to as PHOTO) of stars lying in the annulus between $3.5' < r < 6'$ from the cluster center (region AI in Buonanno et al. 1994). In this annulus all stars down $V \sim 22$ have been measured. The CCD data cover a field of view $7' \times 7'$ roughly centered on the cluster center; stars in the innermost central regions ($r < 20''$) have been not measured. In this sample the deeper exposures (V and I) only reached to $V \sim 20$. In order to ensure an high level (formally 100%) of completeness we include only stars with $V < 17$ lying in the annulus $100''-210''$ from the cluster center. We will refer to this subsample as CCD. The area covered by the CCD subsample and the the others fields in shown Figure 1 of Ferraro et al. (1997b).

In the PHOTO and CCD subsets (in analogy to the *HST* sample) we applied the procedure described in Section 2.2, selecting *bona fide* RGB-SGB-MS members taking all stars within $\pm 5\sigma$ in color from the MRL in the V , $B-V$ and V , $V-I$ CMDs respectively. The CMDs of all stars selected in the three samples (PHOTO, CCD, HST respectively) are shown in Figure 5. For each of these samples we independently derive the LF. Star counts have been corrected using the respective completeness curve: the PHOTO sam-

TABLE 1
MEAN RIDGE LINE FOR THE HST SAMPLE.

<i>V</i>	<i>V</i> – <i>I</i>	<i>V</i>	<i>V</i> – <i>I</i>	<i>V</i>	<i>V</i> – <i>I</i>
RGB					
12.44	1.589	18.16	0.803	15.57	0.775
12.68	1.473	18.26	0.787	15.62	0.731
12.90	1.403	18.33	0.764	15.63	0.684
13.10	1.347	18.37	0.746	15.64	0.631
13.30	1.294	18.42	0.724	15.64	0.585
13.55	1.241	18.47	0.696	15.62	0.272
13.79	1.193	18.52	0.668	15.63	0.219
14.05	1.150	18.57	0.647	15.64	0.184
14.28	1.115	18.62	0.629	15.66	0.146
14.56	1.077	18.70	0.616	15.71	0.105
14.82	1.045	18.78	0.608	15.76	0.079
15.09	1.017	18.86	0.600	15.83	0.043
15.36	0.989	18.98	0.593	15.91	0.008
15.64	0.964	19.10	0.592	15.99	-0.021
15.89	0.939	19.18	0.593	16.10	-0.050
16.21	0.911	19.26	0.595	16.21	-0.069
16.52	0.890	19.38	0.597	16.37	-0.080
16.70	0.879	19.78	0.624	16.54	-0.088
16.94	0.867	20.10	0.654	16.65	-0.091
17.20	0.856	20.30	0.672		
17.36	0.849	20.50	0.693		
17.63	0.836	20.98	0.756		
18.05	0.815	21.34	0.805		

ple has been corrected using Table 7 by Buonanno et al. (1994), the CCD sample (for $V < 17$) is virtually complete, thus no correction has been applied, and the HST sample has been corrected using the completeness curves plotted in Figure 3a,b. In constructing the global LF we considered only the magnitude range where the completeness was greater than 50%. Thus the global LF is restricted to $V \lesssim 21$ by the most incomplete region in the HST sample—the inner region of the WF4 and WF2 cameras (Figure 3a,b).

Since the CCD sample spanned a different magnitude range than the others, we determined a scaling factor to produce a proper match. We followed the procedure explained in Bolte (1994): let $n_{i,k}$ be the number of stars, after the proper completeness correction, in bin i of the sub-sample k , where $k = 1, 2, 3$ indicates the PHOTO, the global *HST*, and the CCD sub-samples, respectively. Thus, for $k = 1, 2$ the resulting LF is simply given by the sum

$$N'_i = \sum_{k=1}^2 n_{i,k}$$

in the range $12 < V < 21$. However, in order to include the CCD sub-sample ($k = 3$) we derived a scaling factor s from the range in magnitude ($12 < V < 17.0$) which is common to all sub-samples:

$$s = \frac{\sum_{k=1}^2 n_{i,k} \sum_i n_{i,k}}{\sum_{k=1}^3 n_{i,k} \sum_i n_{i,k}}$$

so that the number of stars for each bin in the combined LF is

$$N_i = s \times (N'_i + n_{i,k=3}).$$

Table 2 lists the final LF. Column 1 lists the magnitude bins (which are 0.2 mag. in width); column 2 gives N_i , the total scaled number of objects per 0.2 mag; column 3 contains the errors in the N_i . Even though it extends only 2 mag below the turnoff, this LF, including more than 50000 stars, is the most populated LF ever published for a galactic globular cluster.

It is useful to compare our LF to that for M5 obtained by Sandquist et al. (1996, hereafter SBSH), the best previous globular cluster LF. Doing this, it is appropriate to compare sample size in specific parts of the CMD. Our “bright” sample which corresponds to the upper 4.5 mag of the RGB (or $V \leq 17$) contains

944 stars. For such bright stars SBSH were able to work near the cluster center, and their sample in the comparable RGB interval was about 1000 stars. For fainter stars ground based photometry becomes increasingly affected by problems of photometric blends (see SBSH). Blends can be especially insidious when they “move” a star from one part of the LF to another, because this is just the sort of thing one would expect in a breakdown of canonical stellar modeling. To avoid blends only the sparsely populated outer cluster can be used, and it is especially difficult to get adequate samples of the SGB region. Here our blend-free HST sample plays a crucial role. We have 6085 stars brighter than MSTO; SBSH have 3300. In a 0.1 mag bin at turnoff we have 820 stars compared to SBSH’s 280.

4. Results

4.1. Preliminaries

There are certain issues which must be addressed in comparing LFs either with other observational LFs or with theoretical LFs. The first is how the samples are normalized. Beyond this there is some interplay between assumed distance modulus, age, and chemical composition.

4.1.1. Normalization

One must determine a “normalization” factor to adjust for sample size. In recent LF studies (e.g. Stetson 1991, Bolte 1994, Sandquist et al. 1996) both the lower RGB and the main sequence region have been used for normalization. We adopt a different approach normalizing to the total number of stars brighter than the MSTO at $V = 19.10$. Operationally this has the advantage that the turnoff is well defined and because of the large number of stars involved the normalization is not much affected by Poisson statistics. The small imprecision in determining the location of the turnoff ($\lesssim 0.1$ mag) produces only a very small error ($\lesssim 1\%$) in the normalization.

4.1.2. Chemical composition

For M3 Kraft et al. (1992), found $[\text{Fe}/\text{H}] = -1.47$, based on detailed fine abundance analysis of high resolution spectra of red giant stars. However, their study is not fully self-consistent since while stellar analysis was performed using model atmospheres from the grid of Bell et al. (1976, hereafter BEGN),

TABLE 2
LUMINOSITY FUNCTION OF THE GLOBAL SAMPLE (PHOTO+CCD+HST).

V	$\log(N_i)$	σN_i	V	$\log(N_i)$	σN_i
12.70	0.70	0.45	17.50	2.05	1.10
12.90	0.30	0.26	17.70	2.22	1.20
13.10	0.78	0.45	17.90	2.26	1.23
13.30	0.85	0.41	18.10	2.46	1.35
13.50	0.95	0.52	18.30	2.72	1.52
13.70	0.85	0.50	18.50	2.97	1.68
13.90	0.90	0.50	18.70	3.06	1.75
14.10	0.90	0.47	18.90	3.18	1.83
14.30	1.11	0.61	19.10	3.25	1.88
14.50	1.08	0.55	19.30	3.32	1.94
14.70	1.32	0.67	19.50	3.37	1.98
14.90	1.15	0.58	19.70	3.42	2.01
15.10	1.34	0.77	19.90	3.45	2.04
15.30	1.38	0.72	20.10	3.49	2.08
15.50	1.76	0.92	20.30	3.53	2.12
15.70	1.60	0.87	20.50	3.56	2.14
15.90	1.51	0.75	20.70	3.56	2.16
16.10	1.65	0.83	20.90	3.59	2.19
16.30	1.70	0.93	21.10	3.58	2.21
16.50	1.79	0.96	21.30	3.58	2.24
16.70	1.85	1.00	21.50	3.55	2.27
16.90	1.95	1.06	21.70	3.57	2.35
17.10	2.04	1.09	21.90	3.66	2.48
17.30	2.06	1.11			

the reference solar iron abundance was extracted from the empirical Holweger and Müller (1974, hereafter HM) solar model. This inconsistency was resolved by Carretta & Gratton (1997) who use the Kurucz (1993) grid of model atmospheres for both solar and stellar analysis, giving $[\text{Fe}/\text{H}] = -1.34$. The offset with the study of Kraft et al. (from which the observational material was taken) is simply due to the fact that the HM model is ~ 150 K warmer than the BEGN models in the line formation region, explaining the 0.13 dex difference in the derived $[\text{Fe}/\text{H}]$.

Oxygen in red giants can be affected by interior nuclear processing. Indeed, M3 is one of the several clusters with an observed anti-correlation between O and Na along the RGB (see for instance Kraft et al. 1992). This anti-correlation arises because of non-standard mixing on the upper RGB. Therefore, the best estimate for the $[\text{O}/\text{Fe}]$ ratio is that obtained considering only unmixed stars, i.e. giants with $[\text{Na}/\text{Fe}] \approx 0.0$ dex. Using Kraft et al. (1992) we estimate that $[\text{O}/\text{Fe}] = 0.19 \pm 0.04$ dex based on 5 stars.

One typically assumes that the other α -elements (e.g. Kraft et al. 1993) have the same enhancement as O and uses two metallicity parameters, $[\text{Fe}/\text{H}]$ and $[\alpha/\text{Fe}]$, in computing models. For many problems one can get by with just one metallicity parameter using the short cut of Salaris et al. (1993). This makes use of the *global* metallicity ($[\text{M}/\text{H}]$) based on the mass fraction of all elements heavier than helium as compared to solar. They found that scaled solar models with $[\text{Fe}/\text{H}] = [\text{M}/\text{H}]$ mimicked models based on observed $[\text{Fe}/\text{H}]$ with α -enhancement. For M3 $[\text{M}/\text{H}] = -1.2$. So while ideally we would compare M3 data to models with $[\text{Fe}/\text{H}] = -1.34$ and $[\text{O}/\text{Fe}] = 0.2$, a comparison to scaled solar models with $[\text{Fe}/\text{H}] = [\text{M}/\text{H}] = -1.2$ should be an adequate surrogate. Given typical errors in metallicity determinations it is appropriate to explore a region ± 0.3 dex from these values.

4.1.3. Distance modulus and age

In principle, fitting cluster main sequences to sub-dwarfs with precise *Hipparcos* parallaxes should lead to relatively high precision distance moduli. However, M3 was not included in the first round of clusters with distances determined in this way (Reid 1997, Gratton et al. 1997). The main reason was that the fiducial cluster main sequence ridge line (from Ferraro et al. 1997b; CCD97) in the V , $B - V$ plane did not reach deep enough with the photometric accuracy required to apply sub-dwarf fitting to determine distance mod-

uli. However, using an expanded sample of local sub-dwarfs from the newly available Hipparcos catalogue (Carretta et al. 1999a) it is possible to give an estimate for the distance modulus of M3 in the framework of the longer distance scale defined by Gratton et al. (1997) and Reid (1997). With $E(B - V) = 0.02 \pm 0.01$ and $[\text{Fe}/\text{H}] = -1.30$ (to be consistent with reddening and metallicity scales used in Gratton et al. 1997), the true distance modulus for M3 is $(m - M)_0 = 15.13$ (Gratton 1998, private communication, adopting the Ferraro et al 1997b photometry). A cautionary flag to the accuracy of sub-dwarf fitting is set by the fact that different groups using this method do not get the same result (Pont et al. 1997; Reid 1997; Gratton et al. 1997). Small details are important (Carretta et al. 1999a), and systematic effects could leave residual errors of 0.2–0.3 mag in $(m - M)$.

There are other independent estimates of the distance to M3. Cudworth (1979) gives a kinematic distance for M3 of $(m - M)_0 = 14.91$. From the RR Lyrae Sandage and Cacciari (1990) give values of $(m - M)_0$ ranging from 14.81 to 15.00 depending on which metallicity/absolute magnitude relation is adopted for the RR Lyrae. Using the latest metallicity/absolute magnitude determined from Baade-Wesselink distances to field RR Lyrae (Fernley et al. 1998) and our adopted metallicity ($[\text{M}/\text{H}] = -1.2$), we get $(m - M)_0 = 14.86$ (assuming $E(B - V) = 0.01$). In a recent analysis of the RR Lyrae distance scale, De Santis (1996) gives $(m - M)_0 = 15.03$. Marconi et al. (1998) find that $(m - M)_0 = 14.94$ gives a good fit to the LF of the lower main sequence. Ferraro et al. (1999) have recently obtained $(m - M)_0 = 15.05$ within the framework of a homogeneous re-analysis of the evolved sequences of the CMD in a sample of about 60 GGCs. They derived the distance modulus from the comparison of the observed level of the ZAHB (V_{ZAHB}) and the theoretical models computed by SCL97. Their use of synthetic HBs to determine the “observed” V_{ZAHB} is a significant improvement over earlier applications of the same technique.

Given the present state of uncertainty we consider it reasonable to consider $(m - M)_V = 14.8 - 15.2$. The question of age is intertwined with that of distance. The longer distance scales imply smaller ages. For example, with the “sub-dwarf distance” given above and using stellar models from Straniero et al. 1997 (private communication), the corresponding absolute age for M3 is about 12 Gyr. An decrease in $(m - M)$ of 0.07 mag leads to an increase in age of 1 Gyr. Hence

ages of 11–15 Gyr for M3 are not beyond question.

4.2. The Red Giant Branch

The differential LF for our global sample is shown in Figure 6. The dominant determinant of RGB-LF is simply energy conservation via the so-call energy consumption theorem (Renzini & Buzzoni 1986). Basically the number of stars in some interval along the RGB, N_i , depends inversely on the luminosity at that point, $N_i \propto 1/L$. So $\log N_i \propto M_{bol}$, and neglecting bolometric corrections $\log N_i$ should drop linearly with magnitude moving up the RGB just as seen.

Theoretical evolutionary models predict the existence of a “feature” in the RGB called the *LF-bump*. This LF-bump marks the evolutionary stage at which the H-burning shell passes through the composition discontinuity left by the maximum penetration of the convective envelope (Iben 1968, Renzini & Fusi Pecci 1988). As emphasized first by Rood & Crocker (1985), the practical detection of such a feature requires very large RGB samples. Because of this, our global sample gives us the possibility to obtain one of the most precise determinations of the LF-bump.

Models also predict that in the integrated LF the slope changes on either side of LF-bump. The slope change results from the fact that the H-burning shell is moving through a region of increasing hydrogen abundance below the bump and constant hydrogen abundance above the bump. This change in slope can more reliably locate the bump than observations of the bump itself (Rood & Crocker 1985; Fusi Pecci et al. 1990).

In Figure 6 the LF-bump is very well defined in both the differential and integrated LF, and is located at $V = 15.45 \pm 0.05$ (in good agreement with the previous determinations (Buonanno et al. 1994, Ferraro et al. 1997b). Also note in Figure 6 the nomenclature we use to refer to the different branches. Our nomenclature is that of the theorist in which the branches are defined in terms of the supposed interior structure. There is often confusion, in particular, over the term sub-giant branch. To the theorist, and in this paper, SGB refers to the transition region between the MSTO and the lower RGB where the ridge line in the CMD is more horizontal $V = 18.2$ – 18.6 . Structurally this is the branch of thick H-shell burning where the degenerate core develops. For historical reasons observers often refer to stars along the lower-RGB as sub-giants.

We compare our results to two new sets of theoretical evolutionary tracks/isochrones/LFs which use the new OPAL opacities and equation of state (e.g., Rogers & Iglesias 1992). This should offer significant improvement over earlier models particularly for opacity dependent LF features like the LF-bump. The first set (the no-diffusion models described in Straniero et al. 1997, hereafter SCL97) is available for scaled-solar abundances and may be used for any given value of α enhancement with the Salaris et al. (1993) prescription. The second (Bergbush & VandenBerg 1999, hereafter V97) has $[\alpha/\text{Fe}] = 0.3$. The V97 models also include improved color-temperature relations. On the RGB the V97 models utilize a non-Langrangian numerical technique which is not optimal for investigations of the RGB bump. This technique might be expected to smear and perhaps slightly lower the LF-bump.

In Figure 7 the global differential LF is compared to SCL97 and V97 models for $(m - M)_V = 15.03$, age = 12 Gyr. For SCL97 models we took $[\text{Fe}/\text{H}] = [\text{M}/\text{H}] = -1.2$. The V97 models have $[\text{Fe}/\text{H}] = -1.41$ and $[\alpha/\text{Fe}] = 0.3$ which is equivalent to $[\text{M}/\text{H}] = -1.2$. The integrated LF compared to SCL97 is shown in Figure 8. The fits are really quite good with the region of poorest fit at $V \sim 18$ just above the SGB. That the theoretical and observed LFs agree so well for stars brighter than $V \sim 18$ shows that the hydrogen profile in the region $M(r) \sim 0.2$ – $0.4 M_\odot$ is given fairly accurately by canonical models.

The values of $(m - M)$, age, and metallicity which lead to the best LF fit have the virtues of also agreeing well with the longer Hipparcos distance scale with their correspondingly shorter ages and with the abundances obtained by Carretta & Gratton (1998). Furthermore, these parameters fit in well with those obtained from a new re-analysis of the location of the LF-bump in a sample of more than 40 GGCs by Ferraro et al. (1999). They find that the previous discrepancy in the bump location between the observations and models is completely removed using new models and considering the newer global metallicity scale.

The good fit to the LF-bump comes at the expense of some mismatch at the SGB/lower-RGB transition. To explore how varying the parameters affect the fit we must quantify the quality of the fits. Formally we can perform a Chi-squared test computing

$$\chi^2 = \sum_{i=1}^N \left(\frac{\log(N_{\text{observed}})_i - \log(N_{\text{model}})_i}{\log(N_{\text{observed}})_i} \right)^2$$

For the best fit to the entire data set ($13 < V < 20.5$), shown in Figure 7, there is a slightly better agreement with the SCL97 models ($\chi^2_{\text{SCL97}} = 0.11$ and $\chi^2_{\text{V97}} = 0.13$).

One could conceivably prefer parameters which do not give the best overall fit. The factors which determine the luminosity of the “theoretical” LF-bump have been discussed in Fusi Pecci et al. (1990), Chieffi and Gratton (1986) and more recently and extensively in Cassisi & Salaris (1997). The most important factors are the opacity in the $1-2 \times 10^6$ K range and the degree that convective elements undershoot the neutral buoyancy point of the convective envelope. Elsewhere the post-TO LF depends mostly on the rate of fuel consumption (but see §4.3 below), and one might expect it to be a considerably more robust prediction of the models than the location of the LF-bump. Given this one might tolerate some residual error in the LF-bump location to achieve a better fit elsewhere and, thus, exclude the bump region when measuring the quality of the fit. If we do so for the fits shown in Figure 7 we find $\chi^2_{\text{SCL97_xbump}} = 0.01$ and $\chi^2_{\text{V97_xbump}} = 0.02$.

In Figure 9 we explore the effect of varying the distance modulus, age and chemical composition. Since the quality of the fit is essentially the same for SCL97 and V97, we show results only for the SCL97 models. We have found it impossible to fix parameters so that the model fits the SGB region and the LF-bump equally well. The best fit in the SGB region results from a higher age of 14 Gyr. However the good fit in the SGB region brings with it a worse fit for the LF-bump. The fit to the LF-bump can be restored at an age of 14 Gyr by adopting a higher metallicity and $(m - M)$ smaller than we consider plausible (Figure 9b). The upper end of the allowable $(m - M)$ range gives good fit to the LF-bump (Figure 9c) at the expense of a slightly worse fit to the SGB region and a small age (10 Gyr). The Chi-square values both including and excluding the LF-bump region are given in Table 3.

From the χ -values listed in Table 3 we conclude that considering both the two main observables of the LF (the LF-bump and the SGB-rise) we can find a good agreement (with both SCL97 and V97 models) when we take age = 12, $(m - M)_V = 15.03$ and $[M/H] \sim -1.2$ (see Figure 7). On the other hand, if we consider that some residual error still might be present in the theoretical prediction of the LF-bump location, we get the best agreement between theory

and observations if age = 14, $(m - M)_V = 14.80$ and $[M/H] \sim -1.2$ (see Figure 9a).

A full discussion of the age should also bring in the isochrone fits. These are complicated both by the color calibration and the color-temperature relations. Probably because of this our isochrone fits using the ages and distances determined from the LF give no further indication of whether the age of M3 is closer to 12 or 14 Gyr.

4.3. The Lower Red Giant Branch and Sub-Giant Branch

The lower-RGB & SGB LF can be especially interesting. This is the region in which there has been some indication of a breakdown in the canonical models for very low metallicity clusters (Stetson 1991, Bolte 1994) and recently confirmed for M30 (Bergbush 1996, Guhathakurta et al. 1998, Sandquist et al. 1999). It is the region affected by non-canonical assumptions like WIMP energy transport (Faulkner & Swenson 1993, Degl’Innocenti, Weiss, & Leone (1997)), and helium settling (Proffit & Vandenberg 1991, Straniero et al. (1997)), both of which could reduce cluster age estimates. Rapid stellar rotation (Vandenberg, Larsen, & de Propris 1998) and $[\alpha/\text{Fe}]$ could also affect the SGB region of the LF. We illustrate all of these in Figure 11 (see also Figs. 2 & 3 of Vandenberg et al. 1998). The predicted changes are all small, and age differences can mimic these changes.

As shown in Figs. 7 & 8, the theoretical and observed LFs agree well in the SGB region and lower-RGB. Indeed the fits are pretty good under a wide range of assumptions (Figure 9). We should note that for the excess of lower-RGB stars in M30 cited above, the observed LF lies above the lower-RGB at essentially every bin. For M3 our “bad” fits correspond to only one or two mismatched bins. The fits can be essentially perfect (Figure 9a) if we accept some error in the bump location. Basically, there is no indication for a breakdown in the canonical models. SBSH found a similar result for M5.

On the other hand the observational consequences of plausible non-canonical effects are small so even our good fit may not place very tight constraints on their magnitude. We do not attempt to place such constraints now because we feel that a traditional LF analysis may not be the appropriate way to analyze the SGB. By projecting the star count information onto the “magnitude” axis one loses the information

TABLE 3
CHI-SQUARE RESULTS BETWEEN OBSERVATIONS AND SCL MODELS

	$13 < V < 17$	$17 < V < 20.5$	$13 < V < 20.5$
$[\text{M}/\text{H}] = -1.2$			
$(m - M)_V = 15.03$			
age = 12 Gyr	0.101	0.014	0.114
$[\text{M}/\text{H}] = -1.2$			
$(m - M)_V = 14.80$			
age = 14 Gyr	0.194	0.008	0.201
$[\text{M}/\text{H}] = -0.82$			
$(m - M)_V = 14.65$			
age = 14 Gyr	0.103	0.026	0.130
$[\text{M}/\text{H}] = -1.3$			
$(m - M)_V = 15.20$			
age = 10 Gyr	0.112	0.018	0.131

contained in the color distribution of the stars. In a future paper we will report on our efforts to study the distribution “along” the SGB (see for example, Bergbush & VandenBerg 1997), and provide quantitative estimates as to the degree that non-canonical assumptions can be ruled out.

4.4. Below the Main Sequence Turnoff

Below the MSTO the LF primarily probes the stellar initial mass function (IMF) and cluster dynamics. Having been acquired primarily to study post-MSTO evolution, the data we describe in this paper reaches only ~ 2 mag below the turnoff which corresponds to a mass significantly above the lower mass cutoff for main sequence stars. Deeper LFs (based on almost 25,000 stars) exploring this region are presented in Marconi et al. (1998) and Carretta et al. (1999c).

It is widely recognized that stars in dense systems (like GGCs) are subject to energy exchange through stellar encounters and rapidly evolve toward a state of equipartition of energy (so that stars of lower mass will have higher velocities). As a direct consequence low mass stars should have larger average distance from the center and their distribution will be less cen-

trally concentrated than that of higher mass stars. This mass segregation effect is expected to produce an observable effect on the LF if a sufficiently large radial region of the cluster is sampled.

Such mass segregation has already been found in GGCs surveyed by HST: NGC 6397 (King et al. 1995), 47 Tuc (Paresce et al. 1995), M15 (De Marchi & Paresce 1996), NGC 6752 (Ferraro et al. 1997c). Piotto et al. (1997) give an extended discussion of this topic. Mass segregation has been found in M30 using ground based data (Bolte 1989).

Even with our limited MS coverage, we can see evidence for mass segregation in M3. In Figure 12 we show a comparison of the LFs in three separate radial regions: $r < 20''$; $50'' < r < 100''$; $210'' < r < 360''$. As above the LFs have been normalized to the total number of stars brighter than the MSTO. The inner regions show a significant drop of star counts over the magnitude range $V \sim 20 - 21.5$. We interpret the observed depletion as due to the mass segregation effect. The depletion is obvious even in the small interval of masses sampled. The effect shown in Figure 12 cannot be due to residual incompleteness of the samples. In order to completely remove the effect we

would have to assume a level of completeness which is far smaller than the estimated value. For example in the innermost sample $r < 20''$ (which is almost completely contained in the PC) the measured completeness must be almost a factor 2 in error (dropping from 0.8 down to 0.45) in order to remove the effect.

Is the observed decrease in the star counts consistent with the theoretical expectation? In order to derive the relative distribution of stars of different mass at different distances from the cluster center we have used the formula given by King et al. (1995) following the procedure as explained in DeMarchi and Paresce (1996). The faint end of the LF should be depleted in the core region with respect to the outer regions by the factor $f = (\rho_0/\rho_{\text{ext}})^{m_2/m_1-1}$ where ρ_0 and ρ_{ext} are the stellar densities in the core and in the external region respectively, and m_2 and m_1 are the stellar masses at the faint extreme and TO level of the LF, respectively. We use the tables of SCL97 and assume $(m - M)_V = 15.0$ to relate observed magnitudes to mass—the MSTO at $V = 19.1$ corresponds to $M_V \sim 4$ and a mass of $\sim 0.84 M_\odot$, $V = 20.5$ corresponds to $M_V = 5.5$ and a mass of $\sim 0.73 M_\odot$, and $V = 21.9$ corresponds $M_V = 6.95$ and a mass of $\sim 0.61 M_\odot$, respectively.

The spatial densities can be approximated by the Eqn. 5 in King et al. (1995). In the case of M3 the external region lies at $r_{\text{ext}} \sim 290''$, and taking $r_c \sim 30''$ (Djorgovski 1993), we estimate that the ratio $(\rho_0/\rho_{\text{ext}})$ is ~ 900 . Adopting the mass values obtained above, the density of low-mass stars should be a factor $900^{0.13} \sim 2.4$ less than that in the central. This value is compatible with the observed depletion which is $975/548 \sim 1.8$.

We can also explore the stellar initial mass function (IMF) using our data. The IMF is normally approximated by a power-law mass spectrum of the form $\phi(M)dM = M^{-(1+x)}dM$ where $\phi(M)dM$ is the number of stars in the mass range M to $M + dM$. The observed slope of the IMF measured in terms of x should vary with radius in a way consistent with a underlying global slope. To verify this we use the dynamical models of Pryor, Smith, & McClure (1986). We compute x using Eq. 3 of Bolte (1989). The two magnitude intervals used are $18.55 < V < 20.55$ and $20.55 < V < 21.95$. Figure 13 shows the observed x plotted as a function of radius. We see that $x(\text{observed})$ varies r in a way consistent with the $x(\text{global}) \sim 0$. This is close to the value we inferred from our total sample.

5. Summary

We have obtained a V -band luminosity function for the globular cluster M3 using a combination of ground based photographic and CCD observations and *HST* observations of the cluster center. The sample is the largest, most complete LF every obtained for a globular cluster. It is free from the problems of photometric blends which plague ground-based LFs. In the crucial MSTO/SGB region our sample is more than three times larger than previous LFs.

Following a traditional LF function analysis we find no surprises—canonical stellar models seem to fit the data well. In particular,

- The location of the RGB LF-bump agrees well new theoretical models incorporating the OPAL opacities and enhancements of the α -elements. There is no indication of significant “undershooting” by the convective envelope. The best overall fit is achieved with age = 12, $(m - M)_V = 15.03$ and global metallicity $[M/H] \sim -1.2$ (equivalent to $[\text{Fe}/\text{H}] = -1.34$ and $[\text{O}/\text{Fe}] = 0.2$). On the other hand, if we consider that the physics determining the bump location might have more uncertainty than that determining SGB evolution, we might tolerate a worse fit for the bump to achieve a better fit for the SGB. In that case we find age = 14, $(m - M)_V = 14.80$ and $[M/H] \sim -1.2$
- The slope of the integrated LF changes across the LF bump as predicted by the models. This implies that the H-profile (and thus fuel consumed in the earlier stages) is given reasonably accurately by standard models.
- The LF is well fit in the SGB region. There is no indication of a problem with the canonical models as had been earlier found for low metallicity clusters.
- Below the TO we find evidence for a “flat” IMF ($x \approx 0$) and evidence for mass segregation which is well fit by King models.

The two best observed GGC LFs, that of M3 presented here and M5 by SBSH, seem to be a vindication of the quality of theoretical models. In contrast, the anomalous LF of M30 first found by Bolte (1994) has inconveniently persisted in later studies (Bergbusch 1996, Guhathakurta et al. 1998, Sandquist

et al. 1999). Why should the theory work so well in some cases and fail in others? One can explore possible deficiencies in the models as in VandenBerg et al. (1998). However, we feel that the ultimate resolution of the problem lies in the acquisition of more high quality LFs to determine how common anomalous LFs are and what cluster parameters they correlate with.

We thank Don VandenBerg for providing information prior to publication and for very helpful email discussions. RTR & BD are supported in part by NASA Long Term Space Astrophysics Grant NAG 5-6403 and STScI/NASA Grants GO-5969, GO-6804. This research was partially supported by the *Agenzia Spaziale Italiana* (ASI) and by the MURST as part of the project *Stellar Evolution*. FRF acknowledges the *ESO Visiting Program* for its hospitality.

REFERENCES

Bell, R. A., Gustafsson, B., Nordh, H. L., & Olofsson, S. G. 1976, *A&A*, 46, 391

Bergbush, P. A. 1996, *AJ*, 112, 1061

Bergbush, P. A., & VandenBerg, D. A. 1992, *ApJS*, 81, 163

Bergbush, P. A., & VandenBerg, D. A. 1997, *AJ*, 114, 2604

Bergbush, P. A., & VandenBerg, D. A. 1999, in preparation

Bolte, M. 1989, *ApJ*, 341, 168

Bolte, M. 1994, *ApJ*, 431, 223

Buonanno, R., Buscema, G., Corsi, C. E., Ferraro, I., & Iannicola, G. 1983, *A&A*, 126, 278

Buonanno, R., Corsi, C. E., Buzzoni, A., Cacciari, C., Ferraro, F. R., & Fusi Pecci, F. 1994, *A&A*, 290, 69

Carretta, E., Gratton, R. G., Clementini, G., & Fusi Pecci, F. 1999a, *astro-ph* 9902086

Carretta, E., Gratton, R. G., Sneden, C., & Bragaglia, A., 1999b, in *Galaxy Evolution: Connecting the Distant Universe with the Local Fossil Record*, Observatoire de Paris-Meudon, September 1998, in press (*astro-ph*/9812095)

Carretta, E., et al, 1999c, in preparation

Carretta, E., & Gratton, R. G. 1997, *A&AS*, 121, 95

Cassisi, S., & Salaris, M. 1997, *MNRAS*, 285, 993

Castellani, V., Ciacio, F., Degl'Innocenti, S., & Fiorentini, G. 1997, *A&A*, 322, 801

Chieffi, A. & Gratton, R. G. 1986, *Mem. Soc. Astron. It.*, 57, 395

Cudworth, K. M. 1979, *AJ*, 84, 1312

Degl'Innocenti, S., Weiss, A., & Leone, L. 1997, *A&A*, 319, 487

De Marchi G., & Paresce, F. 1996, *ApJ*, 467, 658

De Santis, R. 1996, *A&A*, 306, 755

Djorgovski, S. G. 1993 in *ASP Conf. Ser.* 50, *Structure and Dynamics of Globular Clusters*, ed. S. G. Djorgovski & G. Meylan (Sanfrancisco: ASP), 373

Faulkner, J., & Swenson, F. J. 1993, *ApJ*, 411, 200

Fernley, J., Carney, B. W., Skillen, I., Cacciari, C., & Janes, K. 1998, *MNRAS*, 293, L61

Ferraro, F. R., Fusi Pecci, F., Cacciari, C., Corsi, C.E., Buonanno, R., Fahlman, G. G., & Richer, H.B., 1993, *AJ*, 106, 2324

Ferraro, F. R., Paltrinieri, B., Fusi Pecci, F., Cacciari, C., Dorman, B., Rood, R.T., Buonanno, R., Corsi, C., Burgarella, D., & Laget, M. 1997a, *A&A*, 324, 915

Ferraro, F. R., Carretta, E., Corsi, C., Fusi Pecci, F., Cacciari, C., Buonanno, R., Paltrinieri, B., & Hamilton, D., 1997b, *A&A*, 320, 757

Ferraro, F. R., Carretta, E., Bragaglia, A., Renzini, A., & Ortolani, S. 1997c, *MNRAS*, 286, 1012

Ferraro, F. R., Messineo, M., Fusi Pecci, F., De Palo, A., Straniero, O., Chieffi, A., & Limongi, M., 1999, *AJ*, submitted

Fusi Pecci, F., Ferraro, F. R., Crocker, D. A., Rood, R. T., & Buonanno, R. 1990 *A&A*, 238, 95

Gratton, R. G., Fusi Pecci, F., Carretta, E., Clementini, G., Corsi, C., & Lattanzi, M. 1997, *ApJ*, 491, 749

Guhathakurta, P., Webster, Z. T., Yanney, B., Schneider, D. P., & Bahcall, J. N. 1998, *AJ*, 116, 1757

Holweger, H., & Müller, E. A. 1974, Solar Physics, 39, 19

Holtzmann, J. A., Burrows, C. J., Casertano, S., Hester, J. J., Trauger, J. T., Watson, A. M., & Worthey, G., 1995, PASP, 107, 1065

Iben, I. 1968, Nature, 220, 143

Laget, M., Ferraro, F. R., Paltrinieri, B., & Fusi Pecci, F. 1998, A&A, 332, 93

King, I. R., Da Costa, G. S. & Demarque, P. 1985, ApJ, 299, 674

King, I. R., Sosin, C., & Cool, A. 1995, ApJL, 452, 13

Kraft, R. P., Sneden, C., Langer, G. E., & Prosser, C. F. 1992, AJ, 104, 645

Kraft, R. P., Sneden, C., Langer, G. E., & Shetrone, M. D. 1993, AJ, 106, 1190

Krist, J. 1994, Tiny Tim User's Manual Version 4.0

Kurucz, R. L. 1993, CD-ROM 13 and CD-ROM 18

Marconi, G., Buonanno, R., Carretta, E., Ferraro, F. R., Fusi Pecci, F., Montegriffo, P., De Marchi, G., Paresce, F., & Laget, M. 1998, MNRAS, 293, 479

Piotti, G., Cool, A., & King, I. R. 1997, AJ, 113, 1345

Paresce, F., De Marchi, G., & Jedrzejewski, R. 1995, ApJL, 442, 57

Pont, F., Mayor, M., Turon, C., & VandenBerg, D. A. 1998, A&A, 329, 87

Proffit, C. R., & VandenBerg, D. A. 1991, ApJS, 74, 473

Pryor, C., Smith, G. M., & McClure, R. D. 1986, AJ, 92, 1358

Reid, I. N. 1997, AJ, 114, 161

Reid, I. N. 1998, AJ, 115, 204

Renzini, A., & Buzzoni, A. 1986, in Spectral Evolution of Galaxies, ed. C. Chiosi, A. Renzini (Dordrecht: Reidel), 135

Renzini, A., & Fusi Pecci, F., 1988, ARA&A, 26, 199

Rogers, F. J., & Iglesias, C. A. 1992, ApJ, 401, 361

Rood, R. T., & Crocker, D. A. 1985, in The Production and Distribution of C, N, O Elements, ed. J. Danziger, F. Matteucci, & K. Ajär (Garching: ESO), 61

Sandquist, E. L., Bolte, M., Stetson, P. B., & Hesser, J. E. 1996, ApJ, 470, 910

Sandquist, E. L., Bolte, M., Langer, G. E., Hesser, J. E., & Mendes de Oliveira, C. 1999, ApJ, in press, astro-ph/9810259

Salaris, M., Chieffi, A., & Straniero, O. 1993, ApJ, 414, 580

Stetson, P. B. 1991, in ASP Conf. Ser. 13, The Formation and Evolution of Star Clusters, ed. K. Janes (San Francisco: ASP), 88

Straniero, O., Chieffi, A., & Limongi, M. 1997, ApJ, 490, 425

Trager, S., Djorgovski, S., & King, I. 1993, in Structure and Dynamics of Globular Clusters: ASPCS vol. 50, eds. S Djorgowski & G. Meylan (San Francisco: ASP), 347

VandenBerg, D. A., Larson, A. M., & De Propis, R. 1998, PASP, 110, 98

6. FIGURE CAPTIONS

Fig. 1.— The V , $V - I$ CMD for the HST global sample. The sample contains more than 37,000 stars.

Fig. 2.— Map of the WFPC2 field of view. The circle (at $r \sim 50''$) delineates the INNER and OUTER regions.

Fig. 3.— The smoothed interpolating curves of completeness as a function of V magnitude.

Fig. 4.— The zoomed LF with and without completeness corrections. The Main-Sequence-Turn-Off point is labeled.

Fig. 5.— CMDs of stars selected for the LF in each of the three adopted samples: PHOTO, CCD, HST, respectively.

Fig. 6.— Differential Luminosity Function of the global sample (PHOTO+CCD+HST). The names we use to refer to various parts of the LF are indicated.

Fig. 7.— Differential luminosity function of the global sample compared with theoretical models from SCL97 (panel a) and V97 (panel b). The chosen values for distance modulus, age and chemical composition are indicated.

Fig. 8.— Integrated luminosity function of the global sample compared with theoretical models by SCL97.

Fig. 9.— The differential LF of the global sample is compared with SCL97 theoretical models varying metallicity, distance modulus and age.

Fig. 10.— The LF-bump region of the integrated (panel a) and differential (panel b) LF: The position of the LF-bump is indicated. The solid line is the observed LF. The dashed line is based on SCL97 models. The short dashed lines in (panel a) are straight line fits to the LF above and below the LF-bump and are drawn to aid the eye in seeing the change in slope.

Fig. 11.— The dependence of the SGB LF on WIMPs, He diffusion, $[\alpha/Fe]$.

Fig. 12.— A comparison of the LFs in three separate radial regions: $r < 20''$; $50'' < r < 100''$; $210'' < r <$

$360''$.

Fig. 13.— Comparison between the X value (computed as in Bolte 1989) and the dynamical models from Pryor et al. 1986.

TABLE 4
MEAN RIDGE LINE FOR THE HST SAMPLE.

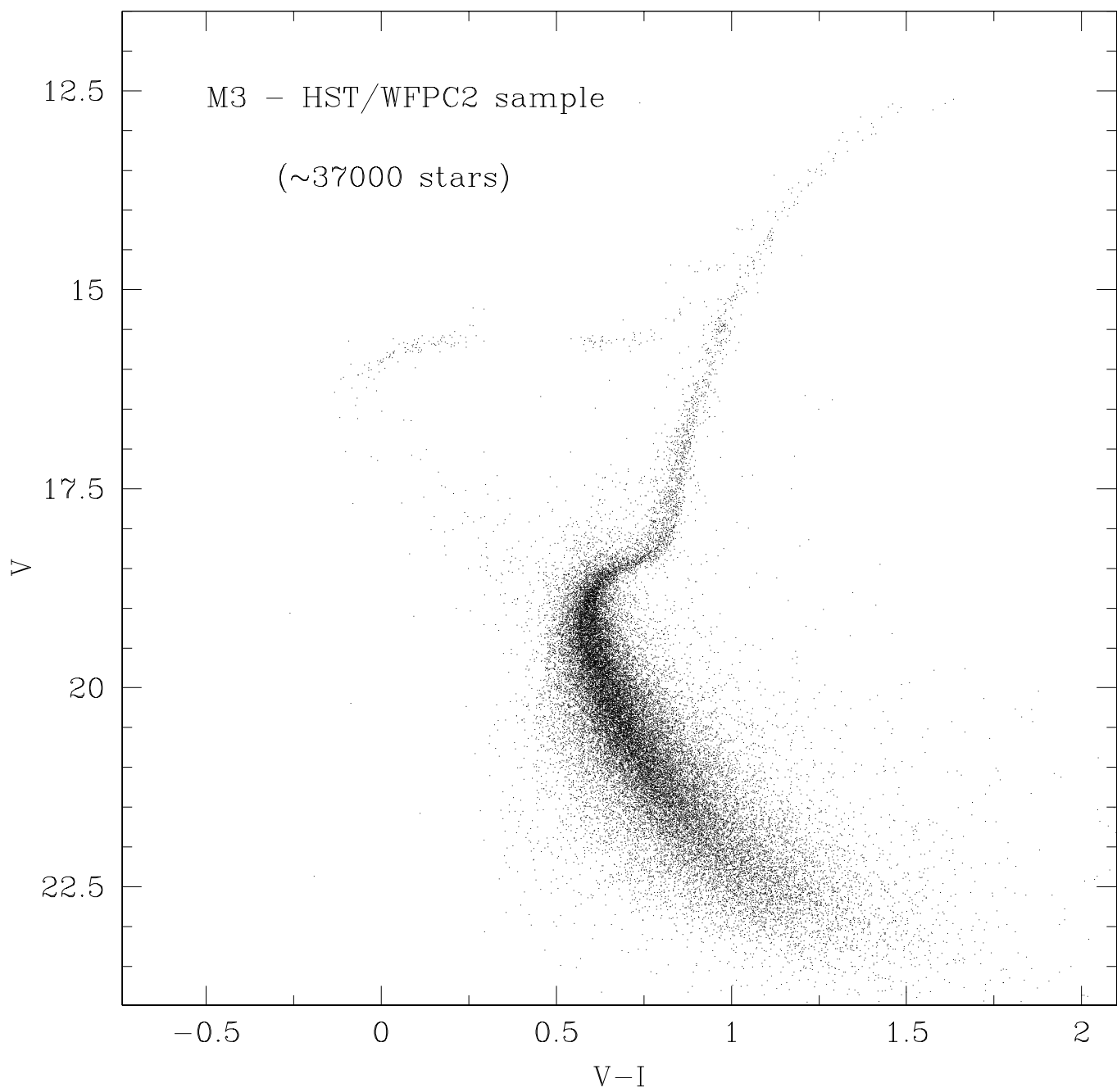
RGB	<i>V</i>	<i>V</i> – <i>I</i>	<i>V</i>	<i>V</i> – <i>I</i>	HB	<i>V</i>	<i>V</i> – <i>I</i>
12.44	1.589		18.16	0.803		15.57	0.775
12.68	1.473		18.26	0.787		15.62	0.731
12.90	1.403		18.33	0.764		15.63	0.684
13.10	1.347		18.37	0.746		15.64	0.631
13.30	1.294		18.42	0.724		15.64	0.585
13.55	1.241		18.47	0.696		15.62	0.272
13.79	1.193		18.52	0.668		15.63	0.219
14.05	1.150		18.57	0.647		15.64	0.184
14.28	1.115		18.62	0.629		15.66	0.146
14.56	1.077		18.70	0.616		15.71	0.105
14.82	1.045		18.78	0.608		15.76	0.079
15.09	1.017		18.86	0.600		15.83	0.043
15.36	0.989		18.98	0.593		15.91	0.008
15.64	0.964		19.10	0.592		15.99	-0.021
15.89	0.939		19.18	0.593		16.10	-0.050
16.21	0.911		19.26	0.595		16.21	-0.069
16.52	0.890		19.38	0.597		16.37	-0.080
16.70	0.879		19.78	0.624		16.54	-0.088
16.94	0.867		20.10	0.654		16.65	-0.091
17.20	0.856		20.30	0.672			
17.36	0.849		20.50	0.693			
17.63	0.836		20.98	0.756			
18.05	0.815		21.34	0.805			

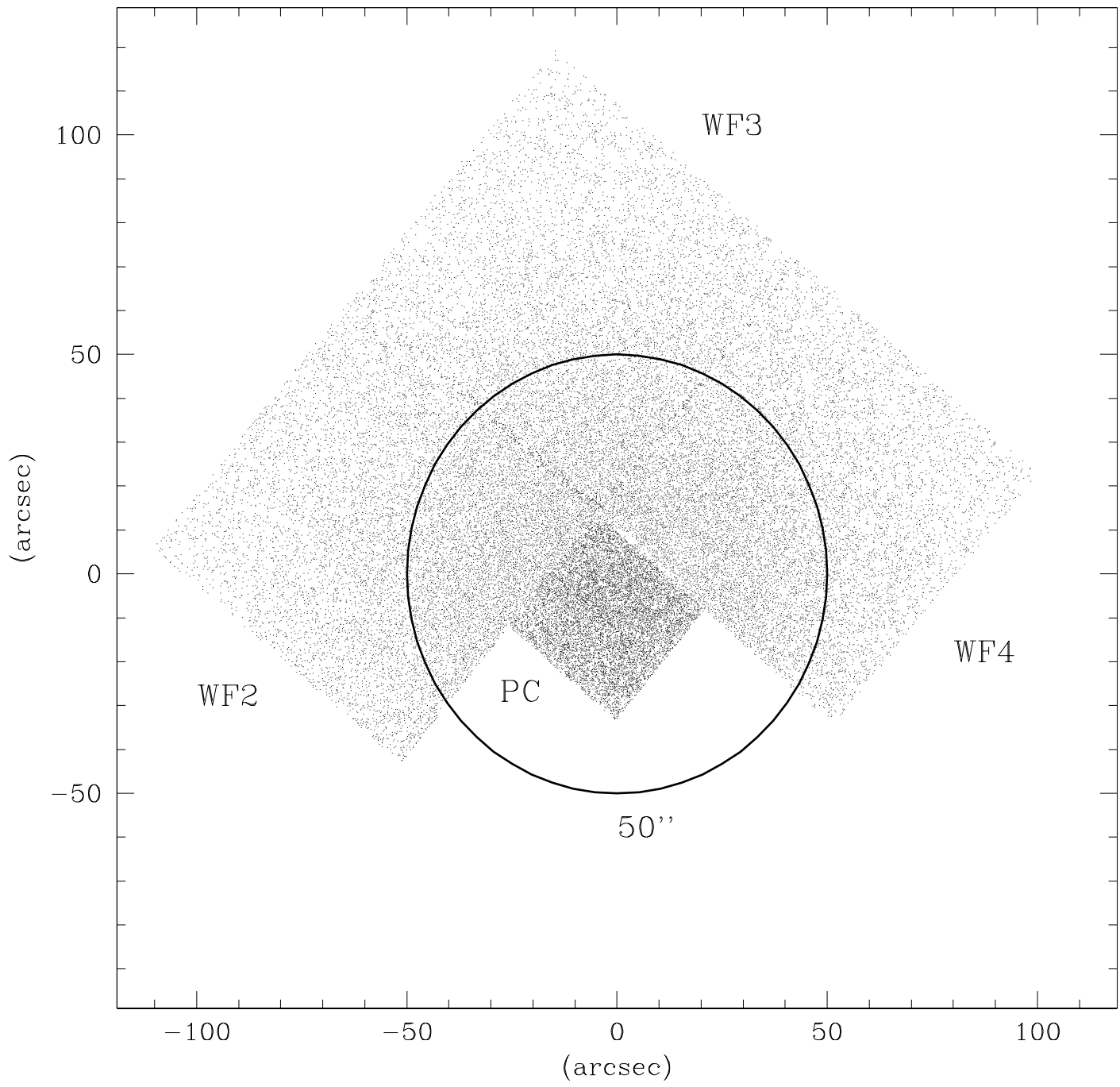
TABLE 5
LUMINOSITY FUNCTION OF THE GLOBAL SAMPLE (PHOTO+CCD+HST).

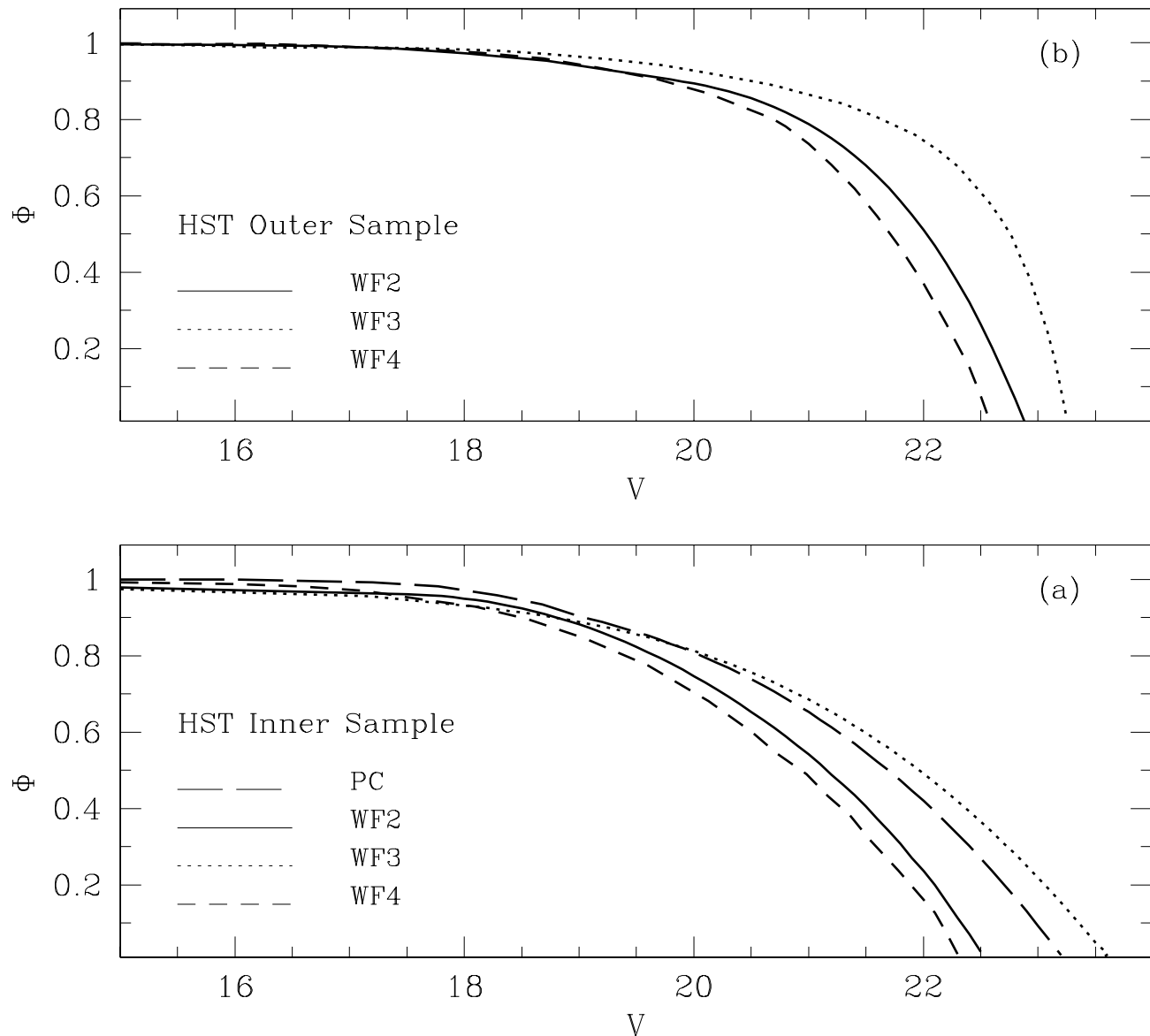
V	$\log(N_i)$	σN_i	V	$\log(N_i)$	σN_i
12.70	0.70	0.45	17.50	2.05	1.10
12.90	0.30	0.26	17.70	2.22	1.20
13.10	0.78	0.45	17.90	2.26	1.23
13.30	0.85	0.41	18.10	2.46	1.35
13.50	0.95	0.52	18.30	2.72	1.52
13.70	0.85	0.50	18.50	2.97	1.68
13.90	0.90	0.50	18.70	3.06	1.75
14.10	0.90	0.47	18.90	3.18	1.83
14.30	1.11	0.61	19.10	3.25	1.88
14.50	1.08	0.55	19.30	3.32	1.94
14.70	1.32	0.67	19.50	3.37	1.98
14.90	1.15	0.58	19.70	3.42	2.01
15.10	1.34	0.77	19.90	3.45	2.04
15.30	1.38	0.72	20.10	3.49	2.08
15.50	1.76	0.92	20.30	3.53	2.12
15.70	1.60	0.87	20.50	3.56	2.14
15.90	1.51	0.75	20.70	3.56	2.16
16.10	1.65	0.83	20.90	3.59	2.19
16.30	1.70	0.93	21.10	3.58	2.21
16.50	1.79	0.96	21.30	3.58	2.24
16.70	1.85	1.00	21.50	3.55	2.27
16.90	1.95	1.06	21.70	3.57	2.35
17.10	2.04	1.09	21.90	3.66	2.48
17.30	2.06	1.11			

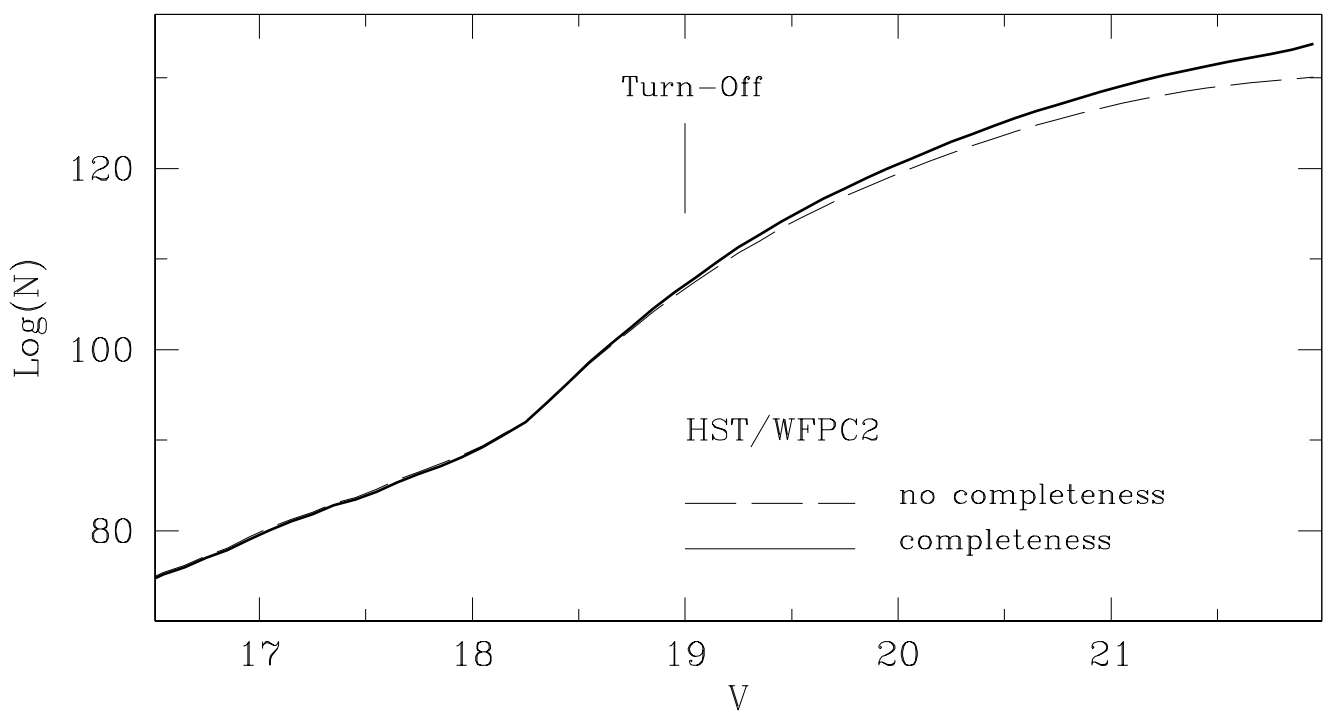
TABLE 6
CHI-SQUARE RESULTS BETWEEN OBSERVATIONS AND SCL MODELS

	$13 < V < 17$	$17 < V < 20.5$	$13 < V < 20.5$
$[\text{M}/\text{H}] = -1.2$			
$(m - M)_V = 15.03$			
age = 12 Gyr	0.101	0.014	0.114
$[\text{M}/\text{H}] = -1.2$			
$(m - M)_V = 14.80$			
age = 14 Gyr	0.194	0.008	0.201
$[\text{M}/\text{H}] = -0.82$			
$(m - M)_V = 14.65$			
age = 14 Gyr	0.103	0.026	0.130
$[\text{M}/\text{H}] = -1.3$			
$(m - M)_V = 15.20$			
age = 10 Gyr	0.112	0.018	0.131









This figure "f5.gif" is available in "gif" format from:

<http://arxiv.org/ps/astro-ph/9905193v1>

